

Performance of handheld probes for Sentinel lymph node detection

Nida Mir

23-08-2021

Supervisors

Prof.Dr.Ir. B. Ten Haken

Dr.Ir. L. Alic

Prof.Dr. L.W.M.M. Terstappen

Dr.Ir. M.M. Horstman - van de Loosdrecht

Magnetic Detection and Imaging group
Faculty of science and technology
University of Twente
Enschede
The Netherlands



UNIVERSITY OF TWENTE | TECHMED CENTRE

Contents

List of Abbreviations	3
Summary	4
Introduction	5
Handheld Probes	8
Sentimag®	8
DiffMag Probe	8
Europrobe 3.2	9
Materials and Methods	10
Probes and Tracers	10
Phantom	11
Experiments	11
Experiment 1: Detection depth	14
Experiment 2: Resolving power	14
Analysis	15
Results	17
Experiment I: Detection depth	19
Experiment II: Resolving Power	20
Discussion and Conclusions	24
References	27
Appendix A	30
Appendix B	31
Appendix C	32
Appendix D	33
Appendix E	35
Appendix F	36

List of Abbreviations

FoM	Floor of Mouth
GMM	Gaussian Mixture Model
LN	Lymph Nodes
OCC	Oral Cavity Cancer
SLNB	Sentinel Lymph Node Biopsy
SPION	Superparamagnetic iron oxide nanoparticle

Summary

Background: Sentinel Lymph Node Biopsy (SLNB) paves an efficient way of resecting Lymph nodes (LNs) with highest chance of containing potential metastases. While avoiding unnecessary, complication laden procedures, it is imperative that this procedure is reliable. In case of Floor of Mouth (FoM) tumors, shine-through phenomenon impacts the visibility and localization of individual nodes, especially those in proximity to the tumor/injection site. Hence, in FoM, SLNBs have not reported very successful results and there is a need to address this gap. With the introduction of Superparamagnetic Iron oxide nanoparticles (SPIONs) the usage of radioactive tracers, the current standard can be avoided. However, it is not known if magnetic handheld probes, i.e., DiffMag and Sentimag® provide efficient solutions for SLNB in FoM tumors.

Method: In this study, the detection depth and resolving power of magnetic handheld probes DiffMag is compared to Sentimag® and gamma probe, Europrobe 3.2. Magtrace and ^{99m}Tc are the tracers used.

Results: The detection depth was determined to be 10 mm, 17mm for Sentimag®, and 12 mm, 19 mm for DiffMag (for 140 µg Fe and 2800µg Fe Magtrace respectively). In comparison the detection depth of Europrobe extends to >120mm and >170 mm (for ≈5.75MBq and ≈23MBq ^{99m}Tc). At 25mm DiffMag and Sentimag® were able to detect two samples (140 µg Fe and 2800µg Fe Magtrace) as separate sources, whereas Europrobe was not able to determine the location of sources clearly at this distance.

Conclusion: DiffMag handheld probe is a better choice for clinical application in FoM SLNB procedures as compared to Sentimag® and Europrobe. The detection depth of DiffMag is sufficient for SLNB procedures while the resolving power is better than Europrobe. Although the resolving power of DiffMag and Sentimag is comparable, DiffMag can lead to faster and less complicated handling in comparison to Sentimag® due to its non-linear magnetic detection mechanism.

Keywords: DiffMag (Differential Magnetometry), Floor of Mouth (FoM) tumors, Handheld Magnetic probe, Handheld Gamma probe, Sentinel Lymph Node Biopsy (SLNB), shine-through phenomenon

Introduction

Head and neck cancer (HNC) is the 8th most common type of cancer in men, and 9th in women [1]. Worldwide, annually more than 650,000 cases of HNC, and 330,000 deaths are reported [2]. In the Netherlands, a figure of 3,000 is estimated [3, 4]. FoM is the second most common site of oral cavity cancer (OCC), accounting for 28%, following tongue cancer (33%). Moreover, the five-year relative survival for FoM (55%) is lowest amongst other OCC [5]. In case of tumors cells first migrate from a primary tumor, metastasizing to (a limited number of) lymph nodes (LNs). Therefore, SLN is defined as the first LN that receive lymphatic drainage from the primary tumor if the tumor has spread. As SLN status predicts the status of the other distant LNs, SLN is important for staging of cancer and prognosis. Metastatic lymph node in the neck is highly important in staging and treatment of the disease [6]. Sentinel Lymph Node Biopsy (SLNB) is performed for investigation of metastasis propagation in the lymphatic system, while ensuring that the process is minimally invasive and excessive nodes are not dissected. This is essential to avoid side effects such as seroma, lymphedema, and numbness. [7-9].

Currently, elective neck dissection (END) and a sentinel lymph node biopsy (SLNB) are the main options for determination of lymphatic status in patients. During END, all regional lymph nodes (LNs) are excised, but this is generally unnecessary, given the absence of metastases in 70% of patients [10]. On the other hand, in SLNB only the sentinel lymph node (SLN – the first draining LN) is excised. This helps avoid overtreatment leading to lower morbidity, and reduced costs. Hence, the National Comprehensive Cancer Network (NCCN) pushed the acceptance of SLNB for NCCN Clinical Practice Guidelines in Oncology of Head and Neck Cancers, and listed decreased morbidity and improve cosmetic outcome as its advantages [11]. Current clinical practice for SLNB uses radioisotope tracer ^{99m}Tc in combinations such as with sulfur colloid, nanocolloid human serum albumin [12], rituximab [13], etc. The tracer may be used with or without blue dye (isosulfan blue, methylene blue (MB) and patent blue). The tracer and blue dye are administered at or near the tumor site where they then drain to the SLN. The radionuclide enables SLN detection by using a gamma probe, while the dye aids in staining the afferent lymph vessel and the node.

SLNB has been found to be as accurate as END in detecting occult LN metastasis (sensitivity 81% vs. 84%, and negative predictive value 93% vs. 93%, respectively), except for floor of mouth (FoM) tumors (sensitivity 63% vs. 92%, and negative predictive value 90% vs. 97%, respectively) [14]. In the study of Alkureishi et al [15] accuracy rates were significantly lower in FoM tumors as compared to other sites in the oral cavity. For the FoM tumors, the SLNB is reported to show lower technical success rates and poorer accuracy [16]. It is reported that the identification of SLN for FoM tumors was 86%, compared with 97% for other tumors as detected using

preoperative lymphoscintigraphy (LSG), and intraoperative use of blue dye/gamma probe. In another study, the sensitivity for FoM tumors was 80%, compared with 100% for other tumor groups [17]. The proximity of the tumor to the draining lymph node basin gives rise to shine-through radioactivity (Figure 1) and scatter, causing difficulties for both preoperative lymphoscintigraphy and intraoperative radiolocalization using gamma probe [18]. This is a direct consequence of the strong signal after injection around the tumor. Consequently, the NCCN dictates additional caution while conducting SLNB around the FoM [11], considering lower sensitivity rates for SLNB 80–86%, as compared to other tumor subsites of oral cavity 93–97%. [15, 19, 20].

Numerous other techniques such as SPECT/CT have been implemented to support detection of SLNs. However these techniques are preoperative, and moreover, are unable to detect LNs existing close to the injection site in the FoM [21]. PET cameras are stated to have higher resolution, but are not as efficient in terms of intraoperative detection as gamma probes [22]. Moreover, Radioisotope has logistic problems, like availability, handling legislative approval for substance disposal, nuclear medicine setup, training requirements, and cost. [23],[24]. Due to the limitations of the radioactive tracer only 60 % of patients in developed countries have access to SLNB procedures, about 5% in China, and even less in the rest of the world [25] . Also, ^{99m}Tc has a 6 h half-life, which limits the timeframe of SLNB.

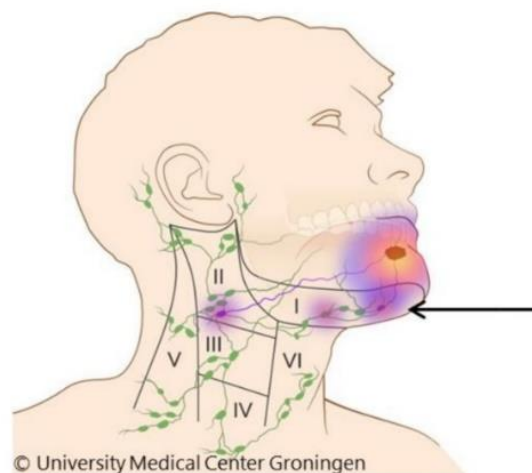


Figure 1: Shine through phenomenon: Radiation flare of the primary tumor overshines the hotspot of a sentinel lymph node in close proximity to the primary tumor (arrow). [26]

As an alternative to radioisotope tracer, magnetic tracer consisting of superparamagnetic iron oxide nanoparticles (SPIONs) is proposed for SLNB. This SPION tracer is a rust-colored solution, consisting of an iron oxide core, along with a biocompatible, polymer coated isolation shell. Clinical studies revealed a non-inferiority of a magnetic SLNB to the radioisotopes in

combination with blue dye [27-33]. Magnetic SLNB has a 97.1% (range 94.4–98.0) mean identification rate, as opposed to a 96.8% as seen in radioisotope technique , and a false negative rate of 5-10% [34].

A magnetic handheld probe Sentimag® developed by Endomag , is used in combination with magnetic tracers. The device is approved by Food and Drug Administration, USA (FDA) for detection of SLNs. Sentimag® relies on linear magnetic detection , which makes it impossible to use the device in combination with metal surgical instruments. At the MD&I Group, UTwente , DiffMag handheld probe has been developed which instead relies on nonlinearity of the magnetization curve of SPIOs . This ensures that the probe is unaffected by magnetic materials proximal to it, during the detection of SPIONs. While DiffMag is resistant to the interference caused by magnetic materials in the surroundings, it's efficiency in SLNB procedures is yet to be tested. Within the context of FoM SLNB not much is known about the performance of magnetic handheld probes and their efficiency to restrict the effect of shine-through phenomenon. Due to the shine-through phenomenon, and its reported effect on the efficiency of SLNB in FoM, it is imperative to improve the perioperative detection of LNs .

To ensure localization of LNs while being unsusceptible to shine-through phenomenon, detection devices must also have better resolving power and optimum detection depth. Therefore, the performance of these probes is of special interest specifically because of occurrence of shine-through phenomenon in FoM tumors, due to the anatomy of LNs. An additional advantage is that use of radioactive tracers and accompanying logistic complications can be avoided. It is presumed that the detection depth of the magnetic handheld probes is favorable for SLNB in FoM. We also conjecture that the handheld probes are more resilient to the shine through effect and can be more effective in localization of SLNs in FoM as compared to radioisotope detection. It is expected that Europrobe has a higher absolute sensitivity, leading to deeper detection, and higher lateral detection distance. This is also expected to have an inverse effect on the spatial resolving power of the device [35]. The aim of this study thus, is to assess the detection depth, and the resolving power of magnetic handheld probes DiffMag, Sentimag® and gamma probe Europrobe. This amounts into the following research questions:

- 1) What is the detection depth of magnetic handheld probe DiffMag compared to Sentimag®, and Europrobe?
- 2) How does the resolving power of DiffMag probe compare to Sentimag® and Europrobe?

Handheld Probes

Sentimag®

Sentimag® (Endomagetics Ltd, UK) is a recently developed magnetic handheld probe for the detection of SPIONs in SLNB. Clinical studies reveal that Sentimag® based SLNB is a feasible alternative to standard radioisotope based SLNB [28, 36]. Sentimag® uses a linear magnetic detection principle, which is sensitive to different types of magnetic signal (e.g., paramagnetism, diamagnetism, ferromagnetism). Consequently, this probe detects all magnetic signals in its proximity, including tissue, metal implants and surgical steel instruments. To partially compensate for this, the probe requires calibration before every measurement, making the process complicated and time consuming. This probe is straight, with a diameter of 18 mm.

DiffMag Probe

DiffMag (MD&I, UTwente) aids in the detection of SPIONs even at smaller quantities, without being affected by the diamagnetic signal contribution of the surrounding tissue. In this method, only a signal specific to the particles is obtained. This specific signature can be found in the strongly nonlinear magnetization characteristics of the SPIO nanoparticles, which contrasts with the linear magnetization curve of tissue (mostly diamagnetic). Differential magnetometry (DiffMag), a patented detection principle, takes advantage of this difference [37]. Figure 2-A illustrates the nonlinearity of the magnetization curve of SPIONs and the linear background signal. To specifically target and localize the SPIO nanoparticles in tissue a series of alternating offset fields is applied observing the derivative of the magnetization curve. The value of this derivative at various points on the curve can be used to distinguish between linear magnetic tissue and SPIONs.

The nonlinearity of the magnetization curve is observable for SPIONs in magnetic fields as low as approximately 1 mT, while the background signal remains linear (Figure 2-A). This allows a low-power solution, ideal for intraoperative use. As DiffMag does not detect the magnetic field of the human body and stationary metal instruments, artefacts resulting from their presence can also be suppressed. Additionally, the magnetic field amplitudes for DiffMag is limited to 5 mT which enables handheld operation with simple hardware [38]. This probe has a diameter of 22 mm.

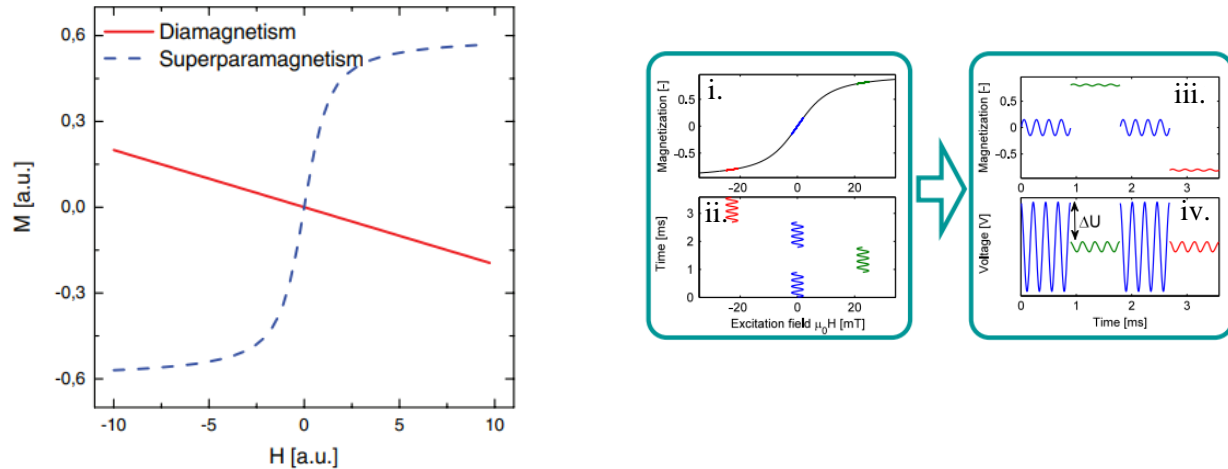


Figure 2 : A) Magnetization versus applied field for an ideal SPIO nanoparticle (blue) and a diamagnetic material (red) [38]. B) Working principle of DiffMag. i) alternating excitation field applied with positive and negative offset field amplitude, ii) Colors in all fields represent the offset field amplitude. Here nonlinear magnetic susceptibility causes a reduced alternating magnetization response during periods with offset field, iii) this is proportional to the amplitude of inductively measured signal, iv) DiffMag voltage ΔU shows the contribution of magnetic nanoparticles in the sample.[39]

Europrobe 3.2

Europrobe 3.2 © (CdTe SOE311 , EuroMedical Instruments, France) is a solid-state ionization-detector probe in which the gamma-ray photons create electron-hole pairs and cause an electrical charge drift to opposite directions using an electric field. This induces signals on electrodes creating an electrical current. The probe has a 60% detector efficiency for ^{99m}Tc (20 - 170 keV). A $5 \times 5 \times 3 \text{ mm}^3$ CdTe or CdZnTe (Cadmium Telluride or CZT) crystal helps in the detection of gamma rays [40]. The probe only has an integral collimator and weighs 140 g which makes handling the probe easy but leads to a weaker resolving power. The crystal volume in the detector affects the sensitivity, as observed in studies. In addition to this, the thickness and stopping power of the detector as well as the energy of the detected radiation determine the sensitivity and hence the detection depth of the device [41]. The probe is angled with the head diameter being 11 mm.

Materials and Methods

This study reports experiments conducted using magnetic probes (Sentimag® (Endomagetics, Cambridge, UK), DiffMag (MD&I UTwente), and gamma-probe (Europrobe 3.2©, CdTe SOE 3211, EuroMedical Instruments, Paris, France). The experiments are conducted using a specifically designed phantom to mimic the anatomical distances between spots of interest (i.e., primary tumor and lymph nodes). The efficiency of handheld probes is evaluated to predict their performance in SLNB of FoM tumors where shine-through phenomenon interferes with the detection of LNs in a near proximity to each other or the injection site.

Probes and Tracers

Sentimag® was used for magnetic detection of magnetic tracer based on its linear magnetization properties (Figure 3-A). DiffMag was used for the detection of magnetic tracer based on a non-linear differential magnetometry principle (Figure 3-B). Clinically available magnetic tracer, Magtrace® (Endomagetics, Cambridge, UK) is used in this study. Magtrace® is CE - and FDA-approved for sentinel node localization.

Europrobe (Europrobe 3.2 ©, CdTe SOE311, EuroMedical Instruments, France) is an ionization-detector probe which is designed to convert the tracer radiation into electrical pulses, Figure 3-C). ^{99m}Tc tracer, in form of ^{99m}Tc -nano colloid human serum albumin, is used as a radioactive tracer in this study. (Figure 3-C)



Figure 3: A) Sentimag® (Endomagetics, Cambridge, UK), B) DiffMag (MD&I UTwente), C) Europrobe© 3.2 (EuroMedical Instruments, Paris, France)

Phantom

Delrin-based (Polyoxymethylene) phantom was designed to mimic the anatomy of nodes in head and neck tumors (Figure 4). The phantom was produced at the MD&I Group, University of Twente. This phantom is non-magnetic and non-reactive to the tracers used. The holes at designated distances were drilled to accommodate pre-decided quantities of the tracer comparable to the tracer quantity trapped into the lymph nodes during magnetic and radioactive SLNB [42]. The phantom consists of 13 rows each containing two small holes (capacity 5 μ l) and one large hole (capacity 500 μ l). The distances between the holes vary between 3 mm and 25 mm [43, 44]. In the phantom a small hole (5 μ l) is representative of a tracer volume accumulated in a lymph node (LN). A bigger hole is representative of the injection sites, with a larger dose of the tracer.

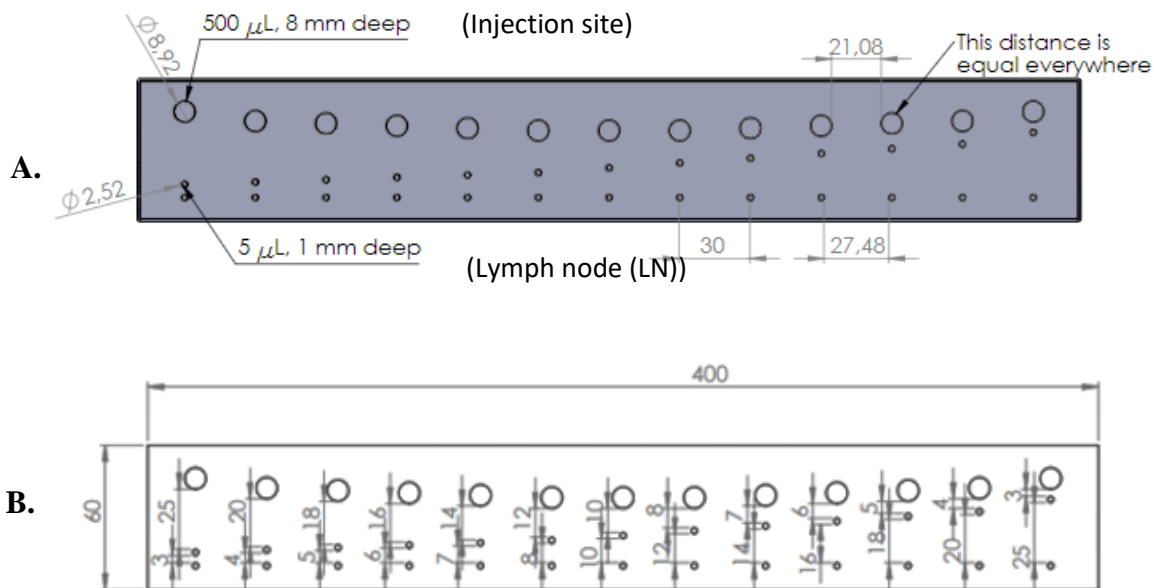


Figure 4: a) Small and big holes dimensions, b) Distances between adjacent holes of phantom

Experiments

The performance of Sentimag, DiffMag and Europrobe was evaluated in two experiments in terms of detection depth (Figure 5-A) and resolving power (Figure 5-B). For each experiment, the tracer (Magtrace or ^{99m}Tc) was pipetted into the individual holes.

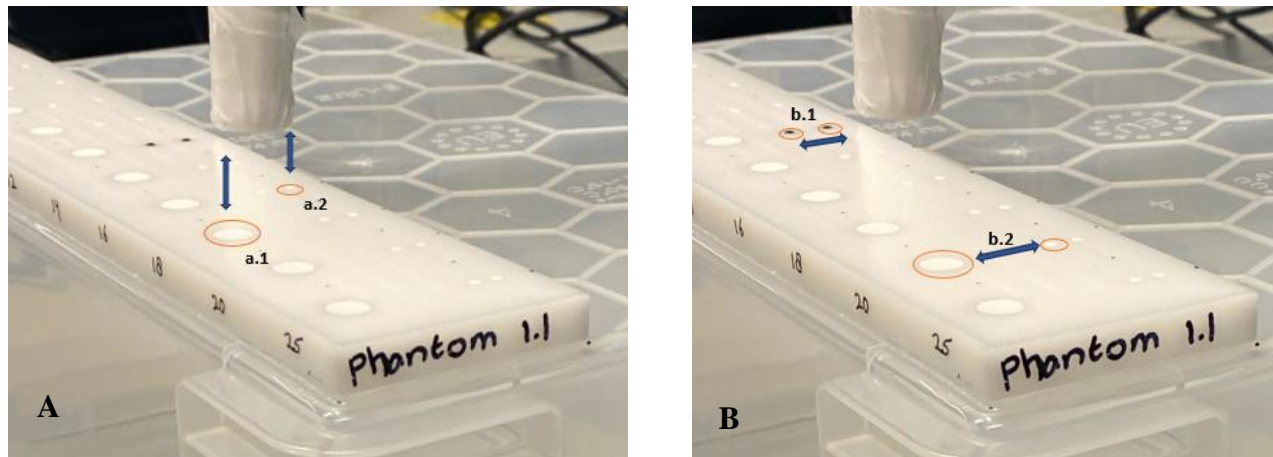


Figure 5: A. Experiment 1: Vertical measurements for detection depth evaluation, B. Experiment 2: Lateral measurements resolving power evaluation

A robotic arm (Meca500, Mecademic, Canada) was programmed to hover at a steady speed across or vertically up the phantom pausing for equal intervals of 8 seconds for Sentimag®, and 5 seconds for DiffMag measurements. For Europrobe measurements, the interval was 10 seconds, and 2 seconds, depending upon the measurement conducted. At each interval, the magnetic/radioactive signal was recorded. The experiments for both tracers (magnetic and radioactive) were conducted with tracer volumes summarized in Table 1.

Table 1 : Tracer quantities used for experiments conducted with Sentimag® and Europrobe 3.2, representing nodes and injection spots

	Sample Volume	Amount	Representing
Magtrace	5 μ l	140 μ g Fe	Node
	400 μ l	2800 μ g Fe	Injection spot
^{99m}Tc	5 μ l	\approx 5.75MBq	Node
	20 μ l	\approx 23MBq	Injection spot

The sample volume of Magtrace used is proportional to amounts of tracer trapped in LNs after draining off from the injection site. This is based on a study stating an LN typically contains $140 \pm 80 \mu\text{g}$ iron for breast cancer patients, after injecting 1.6 mL SPIO tracer Resovist (28 mg (Fe)/mL) [42]. It is also consistent with a recent FoM pilot using Sienna+® magnetic tracer. The 100 μ l Magtrace samples containing 2800 $\mu\text{g}/\text{ml}$ Fe (Endomagnetics Ltd., UK) was used to represent the injection spots based upon 0.4 ml undiluted magnetic tracer administered in four

aliquots in this a pilot study [44]. For experiments measuring the radioactivity of ^{99m}Tc samples, the tracer volume used was $\approx 23\text{MBq}$ for representing an injection spot ($1/4^{\text{th}}$ of the sample used in SLNB), and consequently $\approx 5.75\text{MBq}$ of sample represented an LN.



Figure 6: Experimental setup showing Europrobe3.2, Robotic arm, and phantom (with PMMA)

The Sentimag[®] and DiffMag signals were measured by placing the probes at the closest distance ($\approx 1\text{mm}$) to the phantom surface. For Sentimag[®], the device sensitivity level was set at Level 1 (lowest of three settings available), and data was recorded manually. The probe was calibrated in air at a distance of 30 mm from the magnetic tracer. For DiffMag, PARCEVAL software Rev.250 (developed at MD&I, UTwente) was used to record one magnetic signal in every 0.5 seconds. For radioactive tracer detection the phantom and probe were separated by an additional 17 mm layer of polymethyl-methacrylate (PMMA) transparent thermoplastic to avoid scattering. The probe was placed at $\approx 1\text{mm}$ from the PMMA surface for measurements. Due to high signals acquired at greater tracer quantities detection time for Europrobe was varied between 2 seconds (for $\approx 23\text{MBq}$ ^{99m}Tc), and 10 seconds (for 5.75MBq ^{99m}Tc). Each acquisition was repeated three times to assess the acquisition stability for all devices.

Experiment 1: Detection depth

This experiment evaluates the maximum depth at which the probe can detect the presence of the tracer in air. For both tracers (Magtrace and ^{99m}Tc sample) a single sample was assessed by recording the respective counts starting vertically from the phantom surface with step size of 1mm for Sentimag[®] and DiffMag. For Europrobe, illustrated in Figure 5-A, the step size was set to 5mm (for $\approx 5.7\text{MBq}$) and to 10 mm (for $\approx 23\text{MBq } ^{99m}\text{Tc}$). Tracer signal was measured until the detector only recorded a predetermined background signal. These measurements include observing signals from:

- One small spot
- One big spot

Experiment 2: Resolving power

This experiment evaluates the shortest distance between two tracer samples (Magtrace or ^{99m}Tc sample) at which the position of a target source of activity can be accurately localized, and two target sources of activity which are located relatively close to each other are separated and distinguished indicating no shine-through phenomenon.

The experiments were conducted at a $\approx 1\text{mm}$ from the phantom with a step size of 1mm for Sentimag[®] and DiffMag measurements, and at $\approx 1.7\text{ mm}$ for Europrobe measurements with a step size of 2mm. The signal emitted by the Magnetic /Radioactive tracers and the interaction between neighboring samples was registered (Figure 5-B). The measurements included measuring signals from

- One spot laterally
- Two neighboring small spots
- One small spot, one neighboring big spot

Analysis

The data obtained over two measurements was used to assess the stability of the probes and reproducibility of data using Bland Altman plot. Data acquired over two consecutive measurements by DiffMag was treated as two pairs (for 140 µg Fe sample for Lateral detection depth) and the agreement between the measurements was observed. Data acquired over two measurements, pipetted separately for the same sample volume (140 µg Fe) was analyzed to assess pipetting error. Multiple measurements were conducted using DiffMag and Sentimag (calibrated and uncalibrated) to assess the drift caused when the device is not calibrated.

For analysis of detection depth and resolving power three signals (DiffMag, Sentimag, and Europrobe) were averaged. The averaged signal was normalized between 0 and 1. The depth at which the handheld probes only recorded the background signal from the tracer was ascertained as the detection depth. The results hence obtained were used to compare the detection depth of Sentimag®, DiffMag and Europrobe.

The lateral detection distance is described as the maximum distance from the sample at which the probe can detect the tracer, or in simple words the radius of point spread function. The distance at which the handheld probes only recorded the background signal from the tracer was ascertained as the lateral detection distance.

The resolving power is defined in terms of the distance at which the peaks appear separated, or simply the distance at which the probe is able to accurately determine the location of a source. To analyze the resolving power, Gaussian Mixture Model (GMM) was used to fit a Gaussian curve to the averaged signal and decompose the signal into individual gaussian curves. The highest signal was used as a reference to define the GMM levels at 90%, 75%, 50% (also referred to as FWHM level) and 25%. As illustrated in Figure 7-A, the peaks separate only at 90% of the highest signal level, and do not cross the 75% level.

In case of a big spot adjacent to a small spot replicating an injection spot proximal to LN, a similar approach was used to assess the resolving power. However, in this analysis, the highest level was defined by averaging the highest signal levels obtained through multiple experiments with completely separated peaks. As shown in Figure 7-B, the peaks separate only at the 90% level.

Consequently, a comparison was made to establish the individual resolving power of each device, and their performance opposed to each other.

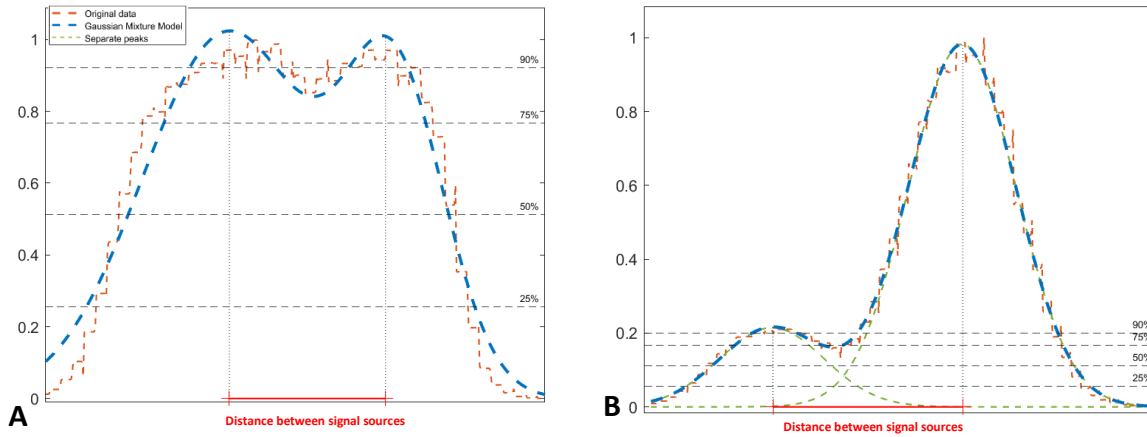


Figure 7: Examples for analysis of signals acquired from A) two small spots, peaks separating at 75% of maximum signal height
 B) One small spot, one big spot, peaks separate at 75% of maximum signal height

Results

Bland Altman plot assessing the probe stability for DiffMag (measured for 140 µg Fe Magtrace) is illustrated in Figure 8-A. The measurements were taken twice for the same sample. The data shows proximity to the mean and is mostly situated (with few outliers) within the limits of agreement in the Bland Altman plot. Figure 8-B shows the GMM fit for the same data sets. The outliers are caused due to data acquired while the probe is in motion as illustrated in raw data plots in Appendix A .

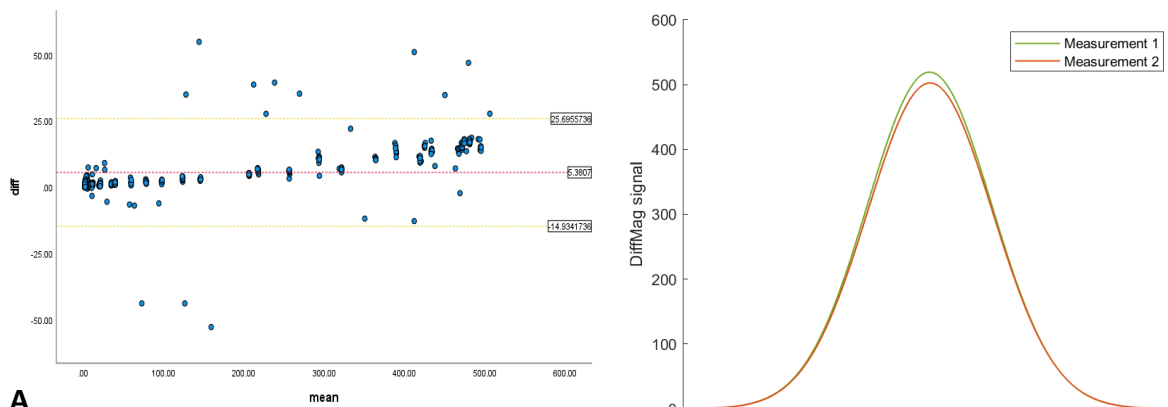


Figure 8:A) Bland Altman plot for two successive measurements for lateral detection distance 140 µg Fe Magtrace DiffMag measurements., B)GMM for the two data sets

The Bland Altman plot for pipetting error analysis is illustrated in Figure 9 . The data sets show proximity to the mean and is mostly situated within the limits of agreement in the Bland Altman plot. The outliers are caused due to data acquired while the probe is in motion.

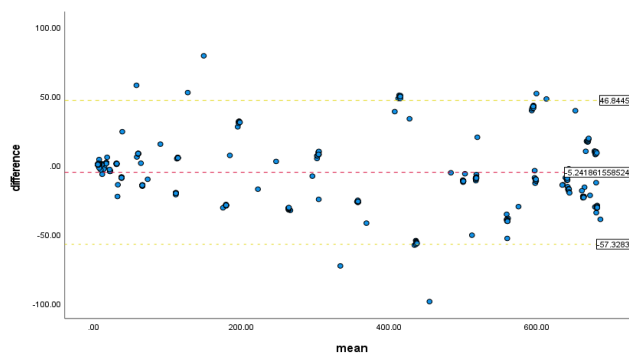


Figure 9) Bland Altman plot for two separate measurements of 140 µg Fe Magtrace using DiffMag to analyze presence of pipetting error.

Figure 10 illustrates repeated measurements taken for detection depth using Sentimag and DiffMag for a constant sample volume at 140 μg Fe. For Sentimag, measurements were repeated with and without calibration to observe the importance of calibration on detection of tracer sample. Without calibrating Sentimag, drift is observed in the recorded signal. The Standard deviation of Sentimag is determined to be 22.85 vs 89.86 at 6mm and 11.57 vs 106.3 at 11mm with and without calibration respectively. On the other hand, for DiffMag Standard deviation was determined to be 7.09 at 6mm and 0.83 at 11mm.

Sentimag also records high background noise, amounting to 84 counts with calibration. In Figure 10-A the minimum recorded background noise is 158 without calibration. Moreover, the background noise for Sentimag changes for each reading, leading to false positive detection. For DiffMag, the background noise is recorded to be 1, as illustrated in Figure 10 B, without calibration.

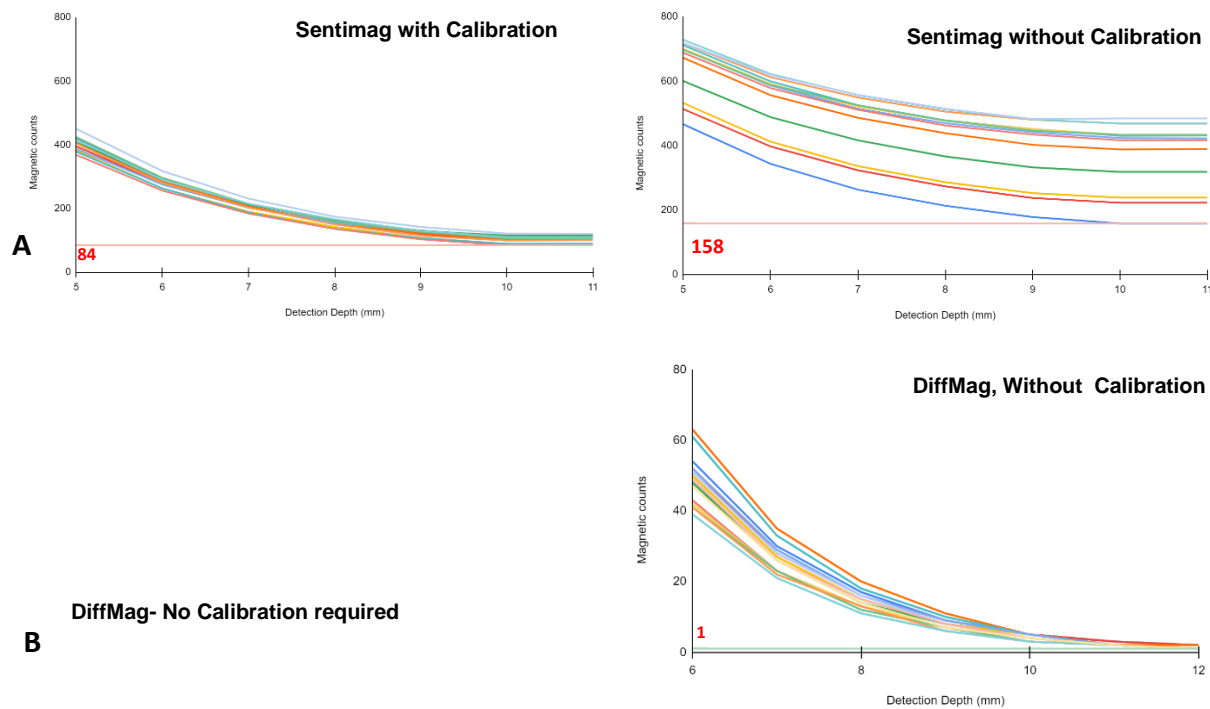


Figure 10 : Repeated measurements for 140 μg Fe Magtrace by A) Sentimag with a calibration performed prior to each acquisition, and Sentimag without calibration and B) for DiffMag without calibration

Experiment I: Detection depth

Figure 11 shows the detection depth for Sentimag® and DiffMag , for Magtrace samples of 140 µg Fe, 2800 µg Fe and Europrobe for ≈5.75MBq, ≈23MBq ^{99m}Tc .

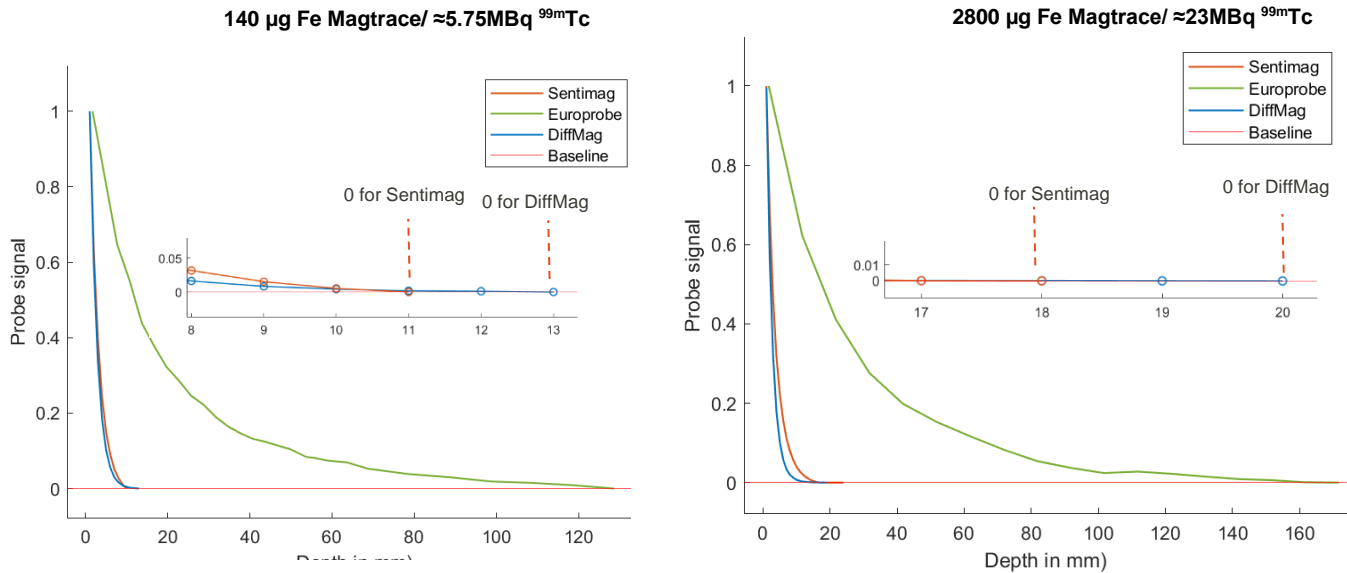


Figure 11: Detection depth (mm) measured for 2800 µg Fe and 140 µg Fe Magtrace by Sentimag® and DiffMag and for ≈23MBq and ≈5.75MBq ^{99m}Tc by Europrobe

Table 2 depicts the detection depth observed for Sentimag, DiffMag and Europrobe, at tracer quantities representing nodes (140 µg Fe or ≈5.75MBq ^{99m}Tc) and injection sites (2800 µg Fe Magtrace or ≈23MBq ^{99m}Tc). The detection depth was determined to be 10 mm for Sentimag® and 12 mm for DiffMag (for 140 µg Fe Magtrace). This parameter additionally was determined to be 17 mm for Sentimag® and 19 mm for DiffMag (for 2800 µg Fe Magtrace) . For Europrobe the detection depth is >120 mm and 170 mm (for ≈5.75MBq and ≈23MBq of ^{99m}Tc respectively).

The detection depth for Sentimag and DiffMag appear similar , and therefore are difficult to visualize in a graph. A Kolmogorov-Smirnov test between the detection depths of Magnetic Probes revealed that there exists a significant difference between the detection depths of the probes (Appendix B).

Table 2. Detection depth for Sentimag, DiffMag and Europrobe for varying tracer quantity

Device/Tracer	Detection depth (mm)	
	140 µg Fe/≈5.75MBq	2800 µg Fe/≈23MBq
Sentimag/ Magtrace	≈10	≈17
DiffMag/ Magtrace	≈12	≈19
Europrobe 3.2/ ^{99m} Tc	>120	>170

Experiment II: Resolving Power

Figure 12 shows the averaged data for lateral detection distance measured using Sentimag® and DiffMag for 140 µg Fe Magtrace and using Europrobe for 5.75MBq ^{99m}Tc samples.

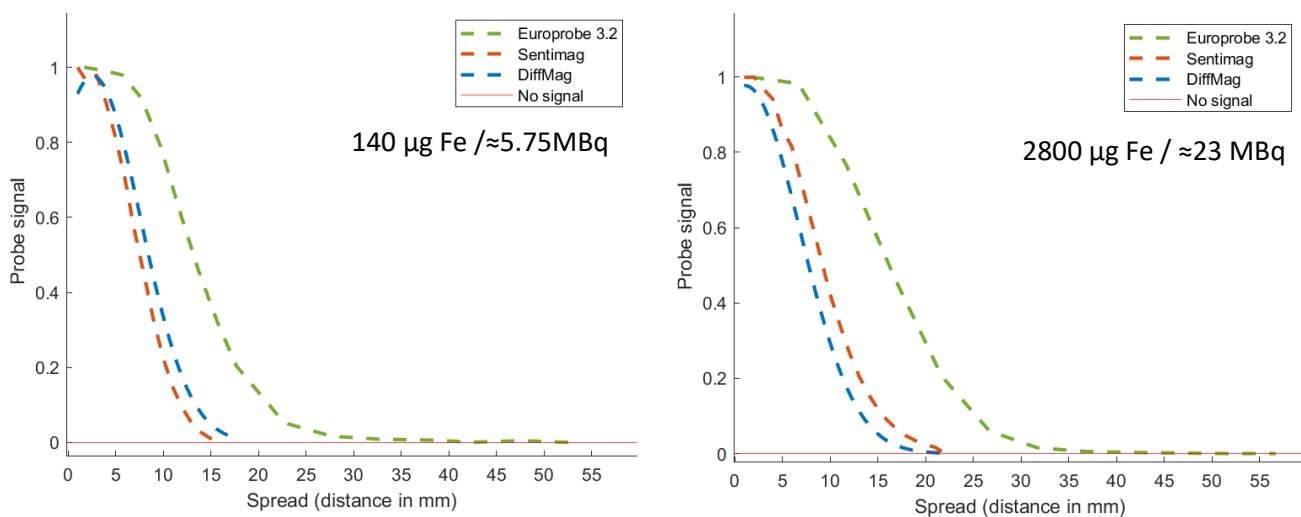


Figure 12: Comparison of Lateral detection distance for Sentimag, DiffMag and Europrobe at 140 µg Fe / ≈5.75MBq and 2800 µg Fe / ≈23 MBq

Table 3 enlists the lateral detection distance for the handheld probes. Beyond the lateral detection distance, the probes only record background signal. The lateral detection distance for Sentimag® is 15 mm, 22 mm, and for DiffMag 16 mm, 21 mm (for 140 µg Fe and 2800 µg Fe Magtrace samples respectively). For Europrobe the lateral detection distance is determined to be 52 mm (for ≈5.75MBq of ^{99m}Tc) and 56 mm (for ≈23MBq samples of ^{99m}Tc).

Table 3: Lateral detection distance summarized for Sentimag, DiffMag and Europrobe

Device/Tracer	Lateral Detection Distance (mm)	
	140 µg Fe/ ≈5.75MBq	2800 µg Fe/≈23MBq
Sentimag/ Magtrace	15	22
DiffMag/ Magtrace	16	21
Europrobe 3.2/ ^{99m} Tc	52	56

For Sentimag® the GMM separates into two peaks at <75% of the maximum averaged signal, for 140 µg Fe Magtrace located 12mm apart, whereas for DiffMag the samples must be 14mm apart. For Europrobe, GMM separates into two peaks at <75% of the maximum averaged signal, for tracer samples (5.75MBq ^{99m}Tc) located 16 mm apart (Figure 13).

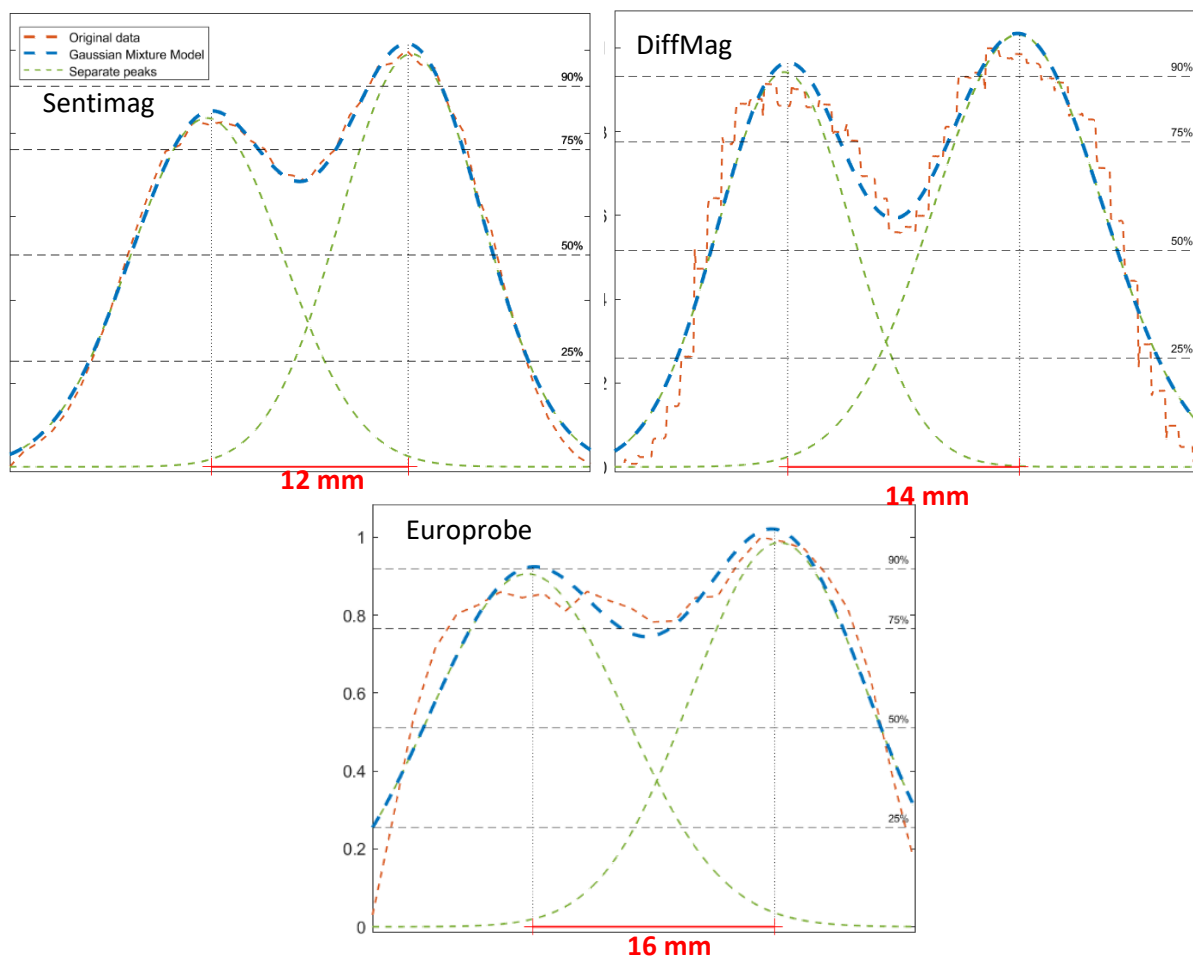


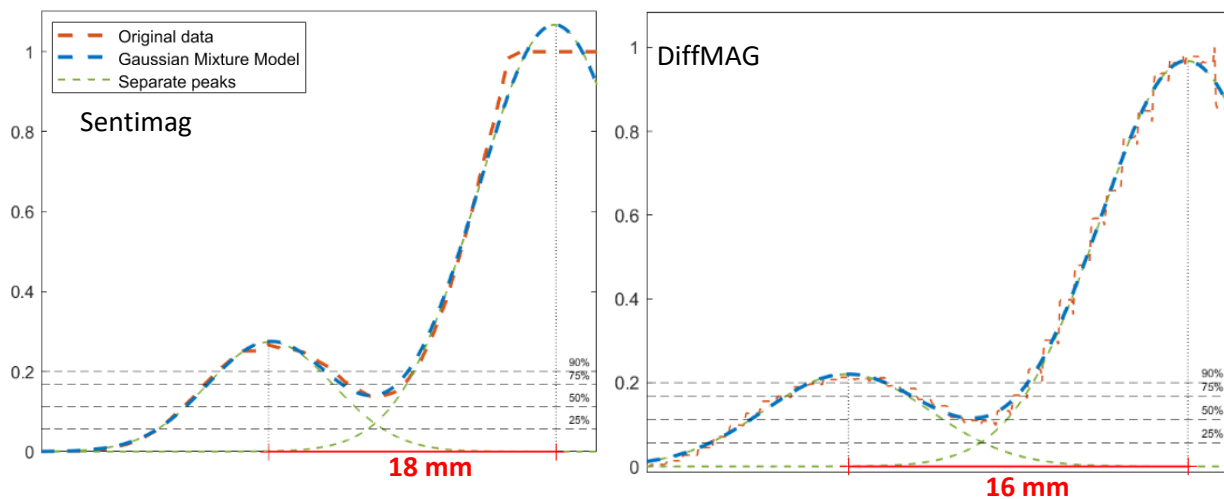
Figure 13: Original data, GMM, and separate peaks as detected by Sentimag® and DiffMag for two small spots (140 µg Fe Magtrace) and Europrobe for (≈5.75MBq ^{99m}Tc). Peaks can be seen separating at 75% of the maximum signal detected

In Table 4 a compilation of the inferences for the resolving powers of probes is summarized. It was found that Sentimag® detects two 140 µg Fe Magtrace samples as two separate peaks at 18mm. DiffMag achieves this resolution at 20mm. Sentimag®, and DiffMag observe two tracer samples as two peaks separating at FWHM at 16mm, whereas Europrobe makes this distinction at 20 mm. For the Europrobe, data for distances > 20 mm in between the samples was not recorded.

Table 4. Resolving power in mm for Sentimag, and Europrobe 3.2, for 90%, 75%, 50% and 25% dips from the peak for two 140 µg Magtrace/ ≈5.75MBq ^{99m}Tc in small spots

Two 140 µg Fe Magtrace / ≈5.75MBq samples			
% of max height	Distance between spots in mm		
	Sentimag	DiffMag	Europrobe 3.2
90%	10	12	-
75%	12	14	16
50%	16	16	20
25%	18	20	-

Figure 14 shows the original data, a Gaussian Mixture Model (GMM) curve and the two individual peaks as fit by the GMM, for one big spot and one small spot, measured by Sentimag, DiffMag and Europrobe. Sentimag® resolves the Magtrace samples representing LN and injection spot at 18 mm for a partition between the peaks dipping below 75% of the highest averaged signal, whereas the same resolution is achieved by DiffMag at 16 mm and Europrobe at 32 mm.



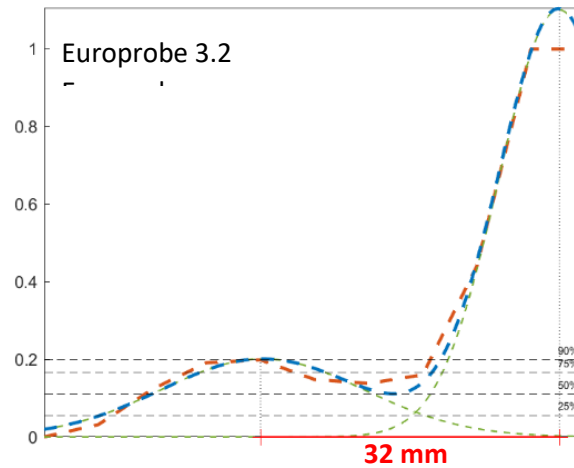


Figure 14: Original data, GMM, and separate peaks as detected by Sentimag® DiffMag and Europrobe for one big spot (2800 µg Fe Magtrace/ ≈23MBq ^{99m}Tc) and one small spot (140 µg Fe Magtrace/ ≈5.75MBq ^{99m}Tc) . Peaks can be seen separating at 75% of the maximum signal detected from the ‘node’ .

Table 5 depicts the inference gathered based on Experiment II. For Europrobe the largest distance measured between the injection spot and the smaller spot was at 32mm. At this distance the peaks were seen separated only at 75% of the highest chosen mean height. On the contrary Sentimag® and DiffMag show better resolving power with the peaks completely separate (< 25% of highest signal) at 25 mm.

Table 5: Resolving power in mm for, Sentimag, and Europrobe 3.2, for 90%, 75%, 50% and 25% dips from the peak, for one big spot (140 µg Fe Magtrace /≈5.75MBq ^{99m}Tc) and one small spot (2800 µg Fe Magtrace / ≈23MBq ^{99m}Tc)

140 µg Fe Magtrace / ≈5.75MBq and 2800 µg Fe Magtrace / ≈23 MBq samples			
% of max height	Distance between spots in mm		
	Sentimag	DiffMag	Europrobe 3.2
90%	16	14	25
75%	18	16	32
50%	20	18	-
25%	25	25	-

Discussion and Conclusions

A lower technical success rate and poorer accuracy are reported for SLNB in FoM tumours [16]. The proximity of the tumor to the draining lymph node basin gives rise to shine-through radioactivity and scatter, and causes difficulties for LN localization during SLNB. [18]. This study compares the performance of DiffMag (nonlinear magnetic handheld probe) for application of SLNB in FoM to the performance of Sentimag® (linear magnetic handheld probe) and Europrobe (Gamma probe), in terms of detection depth and resolving power, for application in SLNB.

For a 140 µg Fe Magtrace sample, the detection depth was assessed to be 10 mm for Sentimag® and 12 mm for DiffMag. For a 2800µg Fe Magtrace sample, the detection depth was assessed to be 17 mm for Sentimag® and 19 mm for DiffMag. In comparison the detection depth of Europrobe extends to >120 mm (for ≈5.75MBq ^{99m}Tc) and >170 mm (≈23MBq ^{99m}Tc). In this study, it was found Sentimag®, and DiffMag can locate two sources accurately (<25% level) at 25mm. At this distance Europrobe makes a distinction only at 90% level, indicating poorer resolving power. This agrees with the finding that intraoperative gamma probe based LN detection can be impaired due to proximity of the LNs to the injection spot [18] resulting in lower success rates of SLNB in FoM as compared to other tumors [17]. This indicates that Sentimag® and DiffMag can help in more efficient detection of LNs in proximity to other LNs, as well as to injection spots as compared to Europrobe.

Lateral detection depth is found to be comparable for the magnetic handheld probes, while significantly larger for Europrobe. Predictably, a larger lateral detection distance translates to a decrease in resolving power. Europrobe, amongst the three handheld probes suffers the consequence of shine-through phenomenon the most, with a very deep detection, but rapid loss of resolving power. This means that Sentimag® and DiffMag have a better resolving power in comparison to Europrobe, along with the advantage of not having to use radioactive tracers. The average depth of mammary lymph node is found to be 3.0 +/- 1.1 cm [45] and is even lesser in FoM [43]. A 98.0% detection rate using Sentimag is recorded per patient as compared to 97.3% using ^{99m}Tc in breast SLNB [32]. Since our study reports greater (and significantly different) detection depth for DiffMag, it can be concluded that the detection depth of DiffMag is sufficient for SLNB in FoM. Additionally, by pressing the probe onto the skin surface, the detection depth of the magnetic probes can be rendered more effective. Moreover, DiffMag also can be used in conjunction to metallic surgical equipment, and in the presence of magnetic materials where the working of Sentimag® is impaired. Furthermore, we have also found that

Sentimag detection is affected if the device is not calibrated which may lead to false positive detections. DiffMag detects only the non-linear signals from the SPIONs and efficiently avoids interference caused by diamagnetic tissue. Therefore, DiffMag does not need constant recalibration like Sentimag®, which can make the detection of SLNs convenient and faster [38].

DiffMag measurements were measured continuously (1 measurement per 0.5 seconds), using PARCEVAL software Rev.250. This introduced error in the data set caused by data points measured while the probe was in motion. To eliminate this error Gaussian Mixture Model (GMM) was used to fit gaussian curves to the average of signals obtained in three consecutive measurements. To maintain uniformity GMM was used to draw inference for resolving power of Sentimag® and Europrobe also. The curves hence fit were used to identify the distance at which the tracer samples can be detected as separate sources. Additionally, in this study, evaluation of the detection depth uses a step size of 1 mm for magnetic probes, and 5-10 mm for gamma probe. This was established as the detection depth of Europrobe is sizeable (> 120 mm), and the experiment was time bound.

A limitation of this study was that the phantom used was slightly curved along its shorter axis (60 mm). This resulted in a difference in signal measured from two equal tracer samples representing two proximal nodes across all measurements. It was confirmed that pipetting error or evaporation of tracer (in magnetic detection experiments) does not contribute to the difference in signal by visually comparing data obtained across all measurements, by all three probes. Additionally, for the FoM, exact locations of the LNs are not known. The widest separation in the spots on the phantom was designed at 25 mm based on the known proximity of LNs to each other in FoM. [43]. Our phantom features spots at fixed distances from each other. Hence the measurements were only conducted at these separations between the samples (Appendix C). Consequently, the resolving power was not assessed at distances not designed in the phantom.

The study found similar resolving power for DiffMag and Sentimag® that can aid in efficient detection of SLNs in FoM. The resolving power of Europrobe was found to be not as accurate as Sentimag and DiffMag. DiffMag however can be established as a better choice for FoM SLNB procedures, as compared to Sentimag® due to comparable resolving power, but with an added advantage of its non-linear detection property. In future, for more precise evaluation a study can be conducted using an improved phantom design for conducting measurements at sample separations which are not possible on our phantom (Appendix C). Information about exact locations and separations between lymph nodes can be used to design such a phantom. Moreover, experiments can be conducted to carry out elaborate comparisons between the probes, by determining the resolving power of Europrobe at various levels and distances (or more) defined in this study. The resolving power can be studied with different detection depths

(Appendix D). Additionally, all measurements using DiffMag in this study were conducted at 2.5kHz. The effect of frequency can be studied with respect to detection depth and resolving power of DiffMag (Appendix E-F) . The magnetic probes' performance can also be compared on basis of their detection depth and resolving power , with other magnetic tracers approved for clinical usage. Additionally, adjustments can be made in the device hardware to reduce the probe size, which may prove more helpful in accurate LN localization during SLNB procedures.

References

1. I. kankercentrum Nederland, h.-h.k., <https://iknl.nl/kankersoorten/hoofd-halskanker>.
2. Bray, F., et al., *Global cancer statistics 2018: GLOBOCAN estimates of incidence and mortality worldwide for 36 cancers in 185 countries*. CA Cancer J Clin, 2018. **68**(6): p. 394-424.
3. Ferlay, J., et al., *Estimates of worldwide burden of cancer in 2008: GLOBOCAN 2008*. Int J Cancer, 2010. **127**(12): p. 2893-917.
4. Jemal, A., et al., *Global cancer statistics*. CA Cancer J Clin, 2011. **61**(2): p. 69-90.
5. van Dijk, B.A., et al., *Trends in oral cavity cancer incidence, mortality, survival and treatment in the Netherlands*. Int J Cancer, 2016. **139**(3): p. 574-83.
6. Layland, M.K., D.G. Sessions, and J. Lenox, *The influence of lymph node metastasis in the treatment of squamous cell carcinoma of the oral cavity, oropharynx, larynx, and hypopharynx: N0 versus N+*. Laryngoscope, 2005. **115**(4): p. 629-39.
7. Krag, D.N., et al., *Surgical resection and radiolocalization of the sentinel lymph node in breast cancer using a gamma probe*. Surg Oncol, 1993. **2**(6): p. 335-9; discussion 340.
8. Giuliano, A.E., et al., *Lymphatic mapping and sentinel lymphadenectomy for breast cancer*. Ann Surg, 1994. **220**(3): p. 391-8; discussion 398-401.
9. Wiechmann, L., et al., *Presenting features of breast cancer differ by molecular subtype*. Ann Surg Oncol, 2009. **16**(10): p. 2705-10.
10. Civantos, F.J., et al., *Sentinel lymph node biopsy accurately stages the regional lymph nodes for T1-T2 oral squamous cell carcinomas: results of a prospective multi-institutional trial*. J Clin Oncol, 2010. **28**(8): p. 1395-400.
11. (NCCN), N.C.C.N., <https://www.nccn.org/>.
12. McMasters, K.M., et al., *Dermal injection of radioactive colloid is superior to peritumoral injection for breast cancer sentinel lymph node biopsy: results of a multiinstitutional study*. Annals of surgery, 2001. **233**(5): p. 676-687.
13. Li, N., et al., *Clinical Evaluation of 99mTc-Rituximab for Sentinel Lymph Node Mapping in Breast Cancer Patients*. J Nucl Med, 2016. **57**(8): p. 1214-20.
14. den Toom, I.J., et al., *Elective Neck Dissection or Sentinel Lymph Node Biopsy in Early Stage Oral Cavity Cancer Patients: The Dutch Experience*. Cancers (Basel), 2020. **12**(7).
15. Alkureishi, L.W.T., et al., *Sentinel node biopsy in head and neck squamous cell cancer: 5-year follow-up of a european multicenter trial*.
16. Civantos, F., R. Zitsch, and A. Bared, *Sentinel node biopsy in oral squamous cell carcinoma*. J Surg Oncol, 2007. **96**(4): p. 330-6.
17. Ross, G.L., et al., *Sentinel node biopsy in head and neck cancer: preliminary results of a multicenter trial*. Annals of surgical oncology, 2004. **11**(7): p. 690-696.
18. Krag, D., et al., *The sentinel node in breast cancer—a multicenter validation study*. New England Journal of Medicine, 1998. **339**(14): p. 941-946.
19. Den Toom, I.J., et al., *Sentinel node biopsy for early-stage oral cavity cancer: The VU University Medical Center experience*.
20. Pedersen, N.J., et al., *Staging of early lymph node metastases with the sentinel lymph node technique and predictive factors in T1/T2 oral cavity cancer: a retrospective single-center study*. Head & neck, 2016. **38**(S1): p. E1033-E1040.
21. Haerle, S.K., et al., *Is there an additional value of spect/ct over planar lymphoscintigraphy for sentinel node mapping in oral/oropharyngeal squamous cell carcinoma?*

22. Vermeeren, L., et al., *A portable gamma-camera for intraoperative detection of sentinel nodes in the head and neck region*.
23. Pouw, J.J., et al., *comparison of three magnetic nanoparticle tracers for sentinel lymph node biopsy in an in vivo porcine model*. 2015.
24. Rescigno, J., J.C. Zampell, and D. Axelrod, *Patterns of axillary surgical care for breast cancer in the era of sentinel lymph node biopsy*. *Ann Surg Oncol*, 2009. **16**(3): p. 687-96.
25. Ahmed, M., A.D. Purushotham, and M. Douek, *Novel techniques for sentinel lymph node biopsy in breast cancer: a systematic review*. *Lancet Oncol*, 2014. **15**(8): p. e351-62.
26. Toom, I., et al., *Sentinel lymph node detection in oral cancer: a within-patient comparison between [99mTc]Tc-tilmanocept and [99mTc]Tc-nanocolloid*. *European Journal of Nuclear Medicine and Molecular Imaging*, 2021. **48**.
27. Houpeau, J.L., et al., *Sentinel lymph node identification using superparamagnetic iron oxide particles versus radioisotope: The French Sentimag feasibility trial*. *J Surg Oncol*, 2016. **113**(5): p. 501-7.
28. Douek, M., et al., *Sentinel node biopsy using a magnetic tracer versus standard technique: the SentiMAG Multicentre Trial*. *Ann Surg Oncol*, 2014. **21**(4): p. 1237-45.
29. Piñero-Madrona, A., et al., *Superparamagnetic iron oxide as a tracer for sentinel node biopsy in breast cancer: A comparative non-inferiority study*. *Eur J Surg Oncol*, 2015. **41**(8): p. 991-7.
30. Rubio, I.T., et al., *The superparamagnetic iron oxide is equivalent to the Tc99 radiotracer method for identifying the sentinel lymph node in breast cancer*. *Eur J Surg Oncol*, 2015. **41**(1): p. 46-51.
31. Ghilli, M., et al., *The superparamagnetic iron oxide tracer: a valid alternative in sentinel node biopsy for breast cancer treatment*. *Eur J Cancer Care (Engl)*, 2017. **26**(4).
32. Thill, M., et al., *The Central-European SentiMag study: sentinel lymph node biopsy with superparamagnetic iron oxide (SPIO) vs. radioisotope*. *Breast*, 2014. **23**(2): p. 175-9.
33. Koops, H.S., et al., *Sentinel node biopsy as a surgical staging method for solid cancers*. *Radiother Oncol*, 1999. **51**(1): p. 1-7.
34. Kim, T., A.E. Giuliano, and G.H. Lyman, *Lymphatic mapping and sentinel lymph node biopsy in early-stage breast carcinoma: a metaanalysis*. *Cancer*, 2006. **106**(1): p. 4-16.
35. Tiourina, T., et al., *Evaluation of surgical gamma probes for radioguided sentinel node localisation*. *Eur J Nucl Med*, 1998. **25**(9): p. 1224-31.
36. Karakatsanis, A., et al., *The Nordic SentiMag trial: a comparison of super paramagnetic iron oxide (SPIO) nanoparticles versus Tc(99) and patent blue in the detection of sentinel node (SN) in patients with breast cancer and a meta-analysis of earlier studies*. *Breast Cancer Res Treat*, 2016. **157**(2): p. 281-294.
37. Nederland, R.v.O.
38. Waanders, S., et al., *A handheld SPIO-based sentinel lymph node mapping device using differential magnetometry*. *Phys Med Biol*, 2016. **61**(22): p. 8120-8134.
39. Molenaar, L., et al. *Sentinel node procedure in prostate and bladder cancer utilizing differential magnetometry: A first patient trial*. 2019.
40. <https://www.em-instruments.com/wp-content/uploads/2018/02/EuroMedical-Instruments-User-Guide-EuroProbe-2018.pdf>, *Surgical Probe Europrobe 3.2 System Operation Manual* january 2018.
41. Pashazadeh, A. and M. Friebe, *Radioguided surgery: physical principles and an update on technological developments*. *Biomedical Engineering / Biomedizinische Technik*, 2020. **65**(1): p. 1-10.
42. Sekino, M., et al., *Handheld magnetic probe with permanent magnet and Hall sensor for identifying sentinel lymph nodes in breast cancer patients*.

43. von Arx T., L.S., *Floor of Mouth. In: Clinical Oral Anatomy.* Springer, Cham, 2017.
44. Eliane R. Nieuwenhuis, B.K., Jurrit J. Hof, Joop van Baarlen, Anke Christenhusz, Remco de Bree, Lejla Alic, *Magnetic tracer uptake within sentinel lymph nodes, an oral cancer patient cohort.* ECHNO-ICHNO2021, 2021.
45. Yip, T.C. and G.N. Ege, *Determination of depth distribution of internal mammary lymph nodes on lateral lymphoscintigraphy.* Clin Radiol, 1985. **36**(2): p. 149-52.

Appendix A

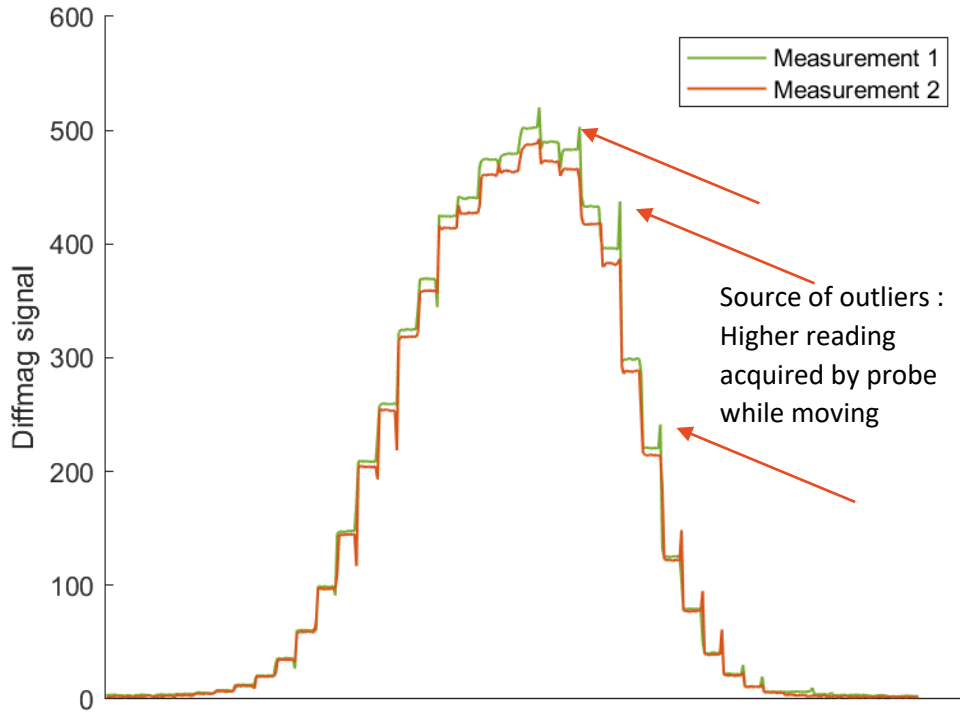


fig 1 : Raw data plots showing source of outliers in Stability Analysis using Bland Altman plot

Appendix B

Detection Depth DiffMag vs Sentimag

T 1: Detection depth measured for DiffMag and Sentimag

Reading	Detection depth in mm	
	DiffMag	Sentimag
1	12	9
2	12	9
3	11	9
4	11	10
5	12	10
6	12	10
7	12	10
8	12	10
9	12	10
10	12	10
11	12	10
12	11	10
13	11	10
14	11	10
15	11	10

Kolmogorov-Smirnov Test for Detection Depth

Hypothesis Test Summary

	Null Hypothesis	Test	Sig. ^{a,b}	Decision
1	The distribution of depths is the same across categories of groups.	Independent-Samples Kolmogorov-Smirnov Test	.000	Reject the null hypothesis.

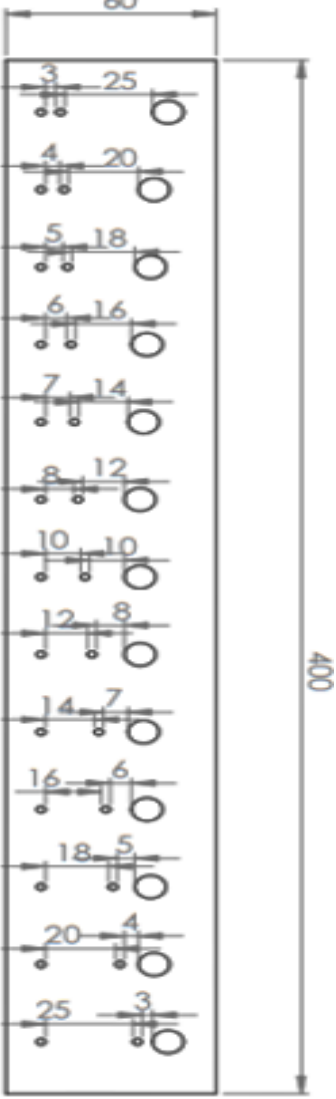
a. The significance level is .050.

b. Asymptotic significance is displayed.

Appendix C

Distances between spots on phantom -

T 2 : Table showing availability of distances between adjacent spots on phantom

	Distance between spots (mm)	Yes	No
	1		
2			•
3		•	
4		•	
5		•	
6		•	
7		•	
8		•	
9			•
10		•	
11			•
12		•	
13			•
14		•	
15			•
16		•	
17			•
18		•	
19			•
20		•	
21			•
22			•
23			•
24			•
25		•	
26			•
27			•
28			•

Appendix D

Effect of Detection Depth on Resolution

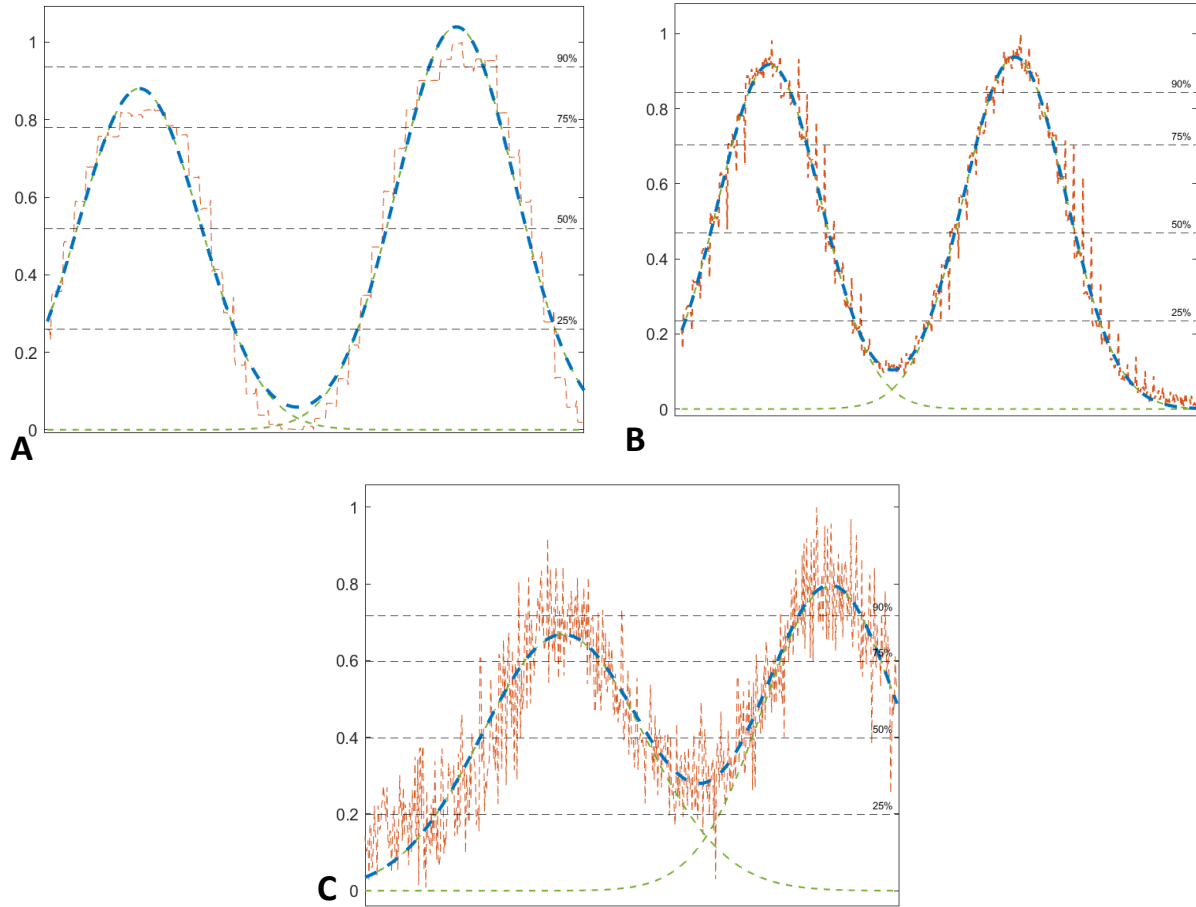


Fig 2: Resolving power of DiffMag at A) 1mm , B) 5mm, C) 10mm , for two 140 μ g Fe Magtrace samples

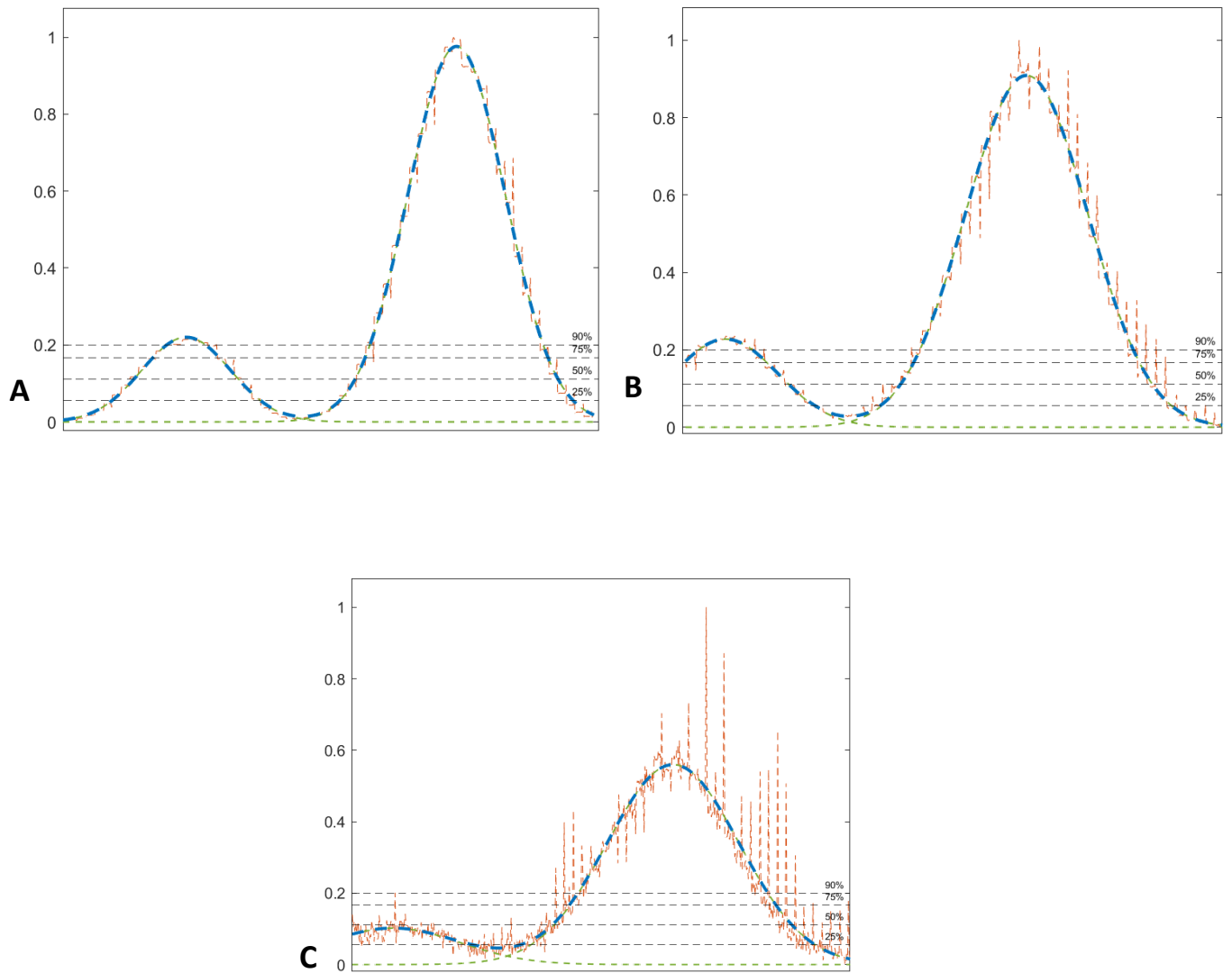


Fig 3:Resolving power of DiffMag at A) 1mm , B)5mm, C)10mm for 140 µg and 2800 µg Fe Magtrace samples

Appendix E

Effect of Frequency on Detection Depth

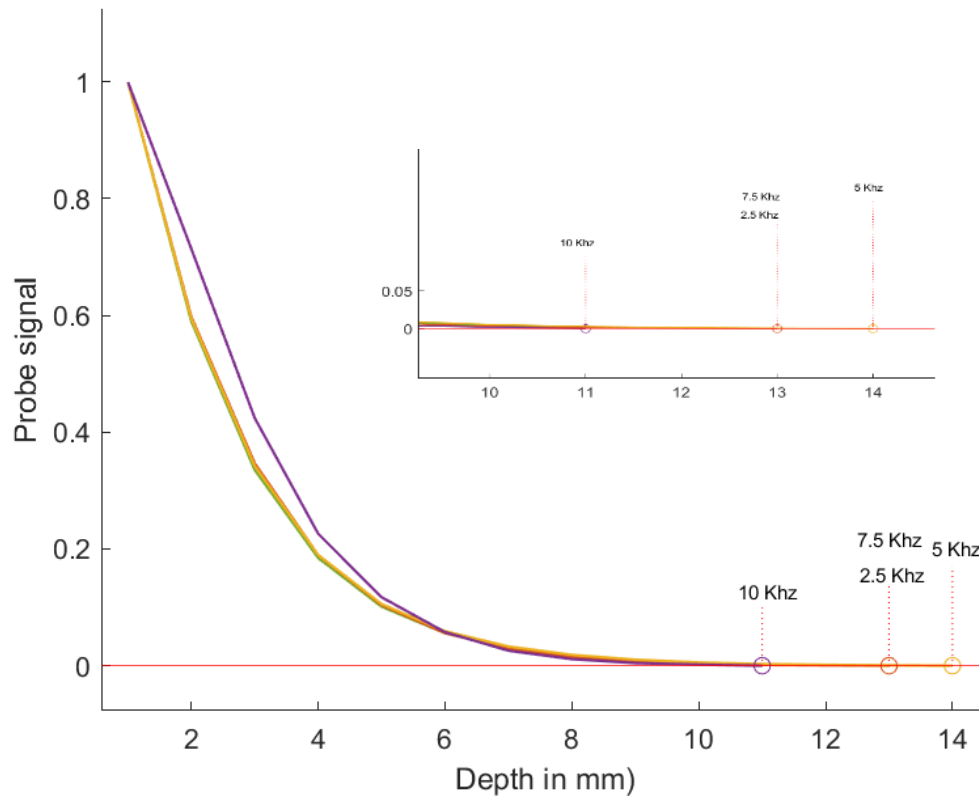


Fig 4: Resolving power of DiffMag at varying alternating frequency

T 3 : Summary of DiffMag at varying frequency

Frequency	Detection depth (mm)
2.5 kHz	≈12
5 kHz	≈13
7.5 kHz	≈12
10 kHz	≈9

Resolving power of alternating

Appendix F

Effect of Frequency on Resolving power

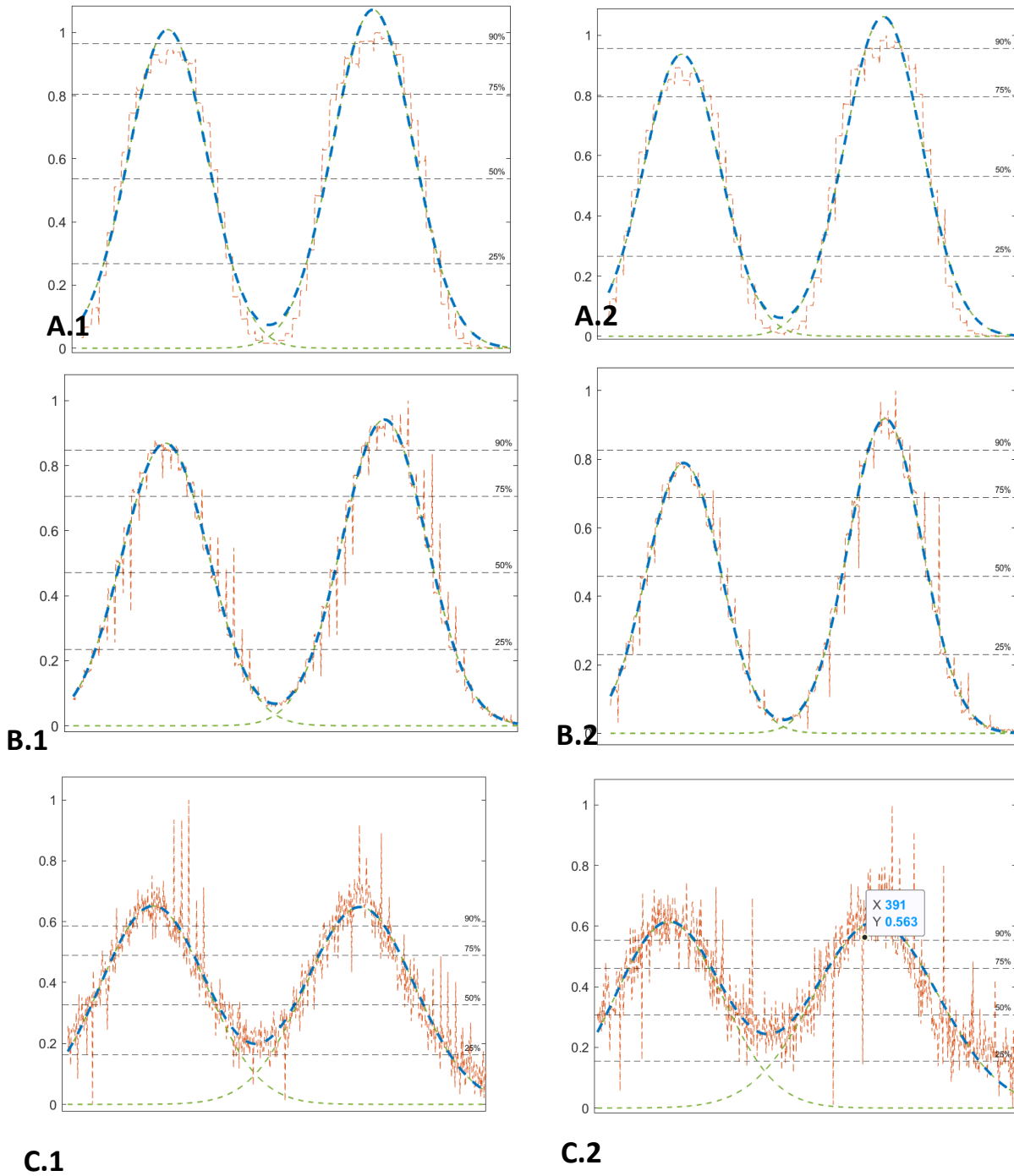


Fig 5 Resolving power of DiffMag with changing depth and frequency : 1mm A.1) 5KHz A.2) 7.5KHz ,at 5mm B.1) 5 kHz , B.2) 7.5 kHz), and 10mm C.1) 5 kHz C.2) 7.5 kHz

